NASA Technical Memorandum 101993

Experimental Investigation of Transonic Oscillating Cascade Aerodynamics

Daniel H. Buffum
Lewis Research Center
Cleveland, Ohio

and

Sanford Fleeter
Purdue University
West Lafayette, Indiana

Prepared for the
27th Aerospace Sciences Meeting
sponsored by the American Institute of Aeronautics and Astronautics
Reno, Nevada, January 9–12, 1989

NASA

Experimental Investigation of Transonic Oscillating Cascade Aerodynamics

Daniel H. Buffum*
National Aeronautics and Space Administration
Lewis Research Center
Cleveland, Ohio 44135
and
Sanford Fleeter**
Thermal Sciences and Propulsion Center
School of Mechanical Engineering
Purdue University
West Lafayette, Indiana 47907

Abstract

Fundamental experiments are performed in the NASA Lewis Transonic Oscillating Cascade Facility to investigate the subsonic and transonic aerodynamics of cascaded airfoils executing torsion mode oscillations at realistic values of reduced frequency. In particular, an unsteady aerodynamic influence coefficient technique is developed and utilized. In this technique, only one airfoil in the cascade is oscillated at a time, with the resulting airfoil surface unsteady pressure distribution measured on one dynamically instrumented reference airfoil. The unsteady aerodynamics of an equivalent cascade with all airfoils oscillating at any specified interblade phase angle are then determined through a vector summation of these data. These influence coefficient determined oscillating cascade data are correlated with: (1) data obtained in this cascade with all airfoils oscillating at several interblade phase angle values; (2) predictions from a classical linearized unsteady cascade model.

Nomenclature

C	airfoil chord
C_p	unsteady pressure coefficient, $p_1/\left(\frac{1}{2}\rho V^2\alpha_1\right)$
$\overline{C}_p$	steady pressure coefficient, $(p_{in}-p_0)/\left(\frac{1}{2}\rho V^2\right)$
$\hat{C}_p^n$	unsteady pressure influence coefficient for n^{th} airfoil
k	reduced frequency, $\omega C/2V$
M	inlet Mach number
p_{in}	inlet static pressure
p_j	j^{th} harmonic of airfoil surface static pressure
S	airfoil spacing
V	inlet velocity
x	chordwise coordinate
y	coordinate normal to chordwise direction
α_0	mean flow incidence angle
α_1	torsional oscillation amplitude
β	interblade phase angle (positive when airfoil n leads airfoil n-1)
γ	stagger angle
ΔC_p	unsteady pressure difference coefficient
ρ	inlet density
ω	airfoil oscillation frequency

Introduction

Oscillating cascade experiments are fundamental to the development of advanced flutter analyses, providing experimental data used to both direct the development of advanced unsteady aerodynamic cascade models and to evaluate these and existing models. Because the ability to predict flutter has not kept pace with advances in the design of turbomachines and advanced propellers, the development of these aerodynamic analyses is of current research interest, references 1-7 for example. However, few experimental results are available at realistic high values of the reduced frequency, particularly in the high subsonic and transonic flow regimes.

The lack of these oscillating cascade data is due to the inherent complexity of the experiments. Measurements must be obtained not only for each steady flow condition and reduced frequency value, but also over a range of interblade phase angles. Typically, because these experiments are so time consuming, results are obtained

* Member AIAA.
** Professor of Mechanical Engineering; Associate Fellow AIAA.

only for several interblade phase angle values. In principle, however, oscillating cascade data may be obtained for all interblade phase angle values through simpler experiments. In particular, when the unsteady disturbances are small, as in the flutter stability problem, an unsteady influence coefficient technique can be utilized. In this technique, only one airfoil in the cascade is oscillated, with the resulting airfoil surface unsteady pressure distributions measured on the oscillating airfoil and its stationary neighbors. The unsteady aerodynamics of an equivalent cascade with all airfoils oscillating at any specified interblade phase angle value is then determined through a vector summation of these influence coefficient data.

Several investigations have been directed at validation of this technique through correlation of unsteady aerodynamic influence coefficient results with corresponding oscillating cascade data acquired with all airfoils oscillating at specified interblade phase angles. Hanamura, Tanaka and Yamaguchi [8] found good results for such experiments in a water channel. Davies and Whitehead [9] performed experiments in an annular cascade at high subsonic inlet conditions, but the measurements were limited to unsteady aerodynamic moment coefficients. The effect of oscillating a single airfoil and three airfoils in cascade at low speed was studied by Tanaka, Yamamoto and Fujimoto [10]. Although a summation of the influence coefficients was not presented, the technique appears promising in regions of attached flow. For a subsonic compressible flow field, Buffum and Fleeter [11] found good correlation of airfoil surface unsteady pressure distributions obtained via influence coefficients and the corresponding interblade phase angle data.

In this paper, the steady and unsteady aerodynamics of a cascade of biconvex airfoils executing torsion mode oscillations are investigated for both subsonic and transonic flow fields. This is accomplished by obtaining fundamental data in the NASA Lewis Transonic Oscillating Cascade Facility. Detailed steady airfoil surface pressure distributions quantify the mean flow field. Unsteady airfoil surface pressure influence coefficients are measured for one airfoil oscillating at realistic values of reduced frequency. These influence coefficients are summed vectorally for correlation with data obtained with all airfoils oscillating at specified interblade phase angle values. The associated unsteady pressure difference data are also correlated with the predictions of a linearized subsonic oscillating cascade analysis.

Influence Coefficient Technique

Figure 1 depicts the two-dimensional finite cascade representation of a rotor blade row. For a given mean flow field and reduced frequency of oscillation, and assuming small unsteady disturbances, the cascade unsteady aerodynamics may be expressed as linearly combined influence coefficients which can be determined both experimentally and analytically.

Consider a finite airfoil cascade with $2N+1$ airfoils executing constant amplitude harmonic oscillations with a constant interblade phase angle β. The unsteady airfoil surface pressure, expressed as a pressure coefficient $C_p(x)$ acting at a point on the reference airfoil (airfoil 0 in Figure 1), can be expressed as a Fourier series

$$C_p(x,\beta) = \sum_{n=-N}^{N} \hat{C}_p^n(x) e^{in\beta} \qquad (1)$$

where $\hat{C}_p^n$ are the complex unsteady aerodynamic pressure influence coefficients. Thus these influence coefficients define the unsteady pressure coefficient developed on the reference airfoil due to the motion of airfoil n with all of the other airfoils stationary.

Oscillating Cascade Facility

The NASA Lewis Transonic Oscillating Cascade Facility, Figure 2, combines a linear cascade wind tunnel, capable of test section inlet Mach numbers approaching unity, with a high speed mechanical drive system which imparts controlled torsional oscillations to any or all of the airfoils. Air drawn from the atmosphere passes through a smoothly contracting inlet section, into a constant area 9.78 by 19.21 cm test section and then through a diffuser and exhaust header. The flow rate is controlled by two valves located in the header. Upstream of the test section, a partitioned bleed system applies suction to the end wall boundary layers, thus reducing end wall viscous effects. Suction is also applied through tailboard slots to reduce effects due to the upper and lower cascade walls.

To obtain realistic values of the reduced frequency, the mechanical drive system must provide high frequency controlled oscillations of the airfoils. Nine barrel cams, each with a six cycle sinusoidal groove machined into its periphery, are mounted on a common rotating shaft driven by a 74.6 kW electric motor. Connecting arms, joined to one end of each airfoil by trunnions, have buttons on the opposite end to follow the camshaft. The amplitude of the airfoil motion is 1.2 degrees, dictated by the cam and follower geometry. For all of the airfoils oscillating, different interblade phase angle oscillations are achieved by rotating the cams to new relative positions. In this

investigation, the maximum airfoil oscillatory frequency is 350 Hz, corresponding to a reduced frequency of 0.39 with a 0.65 cascade inlet Mach number.

Airfoils and Instrumentation

The cascade is comprised of nine uncambered biconvex airfoils with a chord of 7.62 cm, a thickness-to-chord ratio of 0.076, a solidity of 1.3 and a 53 degree stagger angle. The radius of curvature of both airfoil surfaces is 27.4 cm, with the leading and trailing edges rounded with a 0.025 cm radius of curvature. The airfoils are supported by two midchord trunnions, resulting in a midchord elastic axis location.

Steady airfoil surface pressure distributions are measured with conventional static pressure taps. There are sixteen chordwise measurement locations, with four additional taps to assure the spanwise uniformity of the pressure distribution. Rows of sidewall static pressure taps located upstream and downstream of the cascaded airfoils, Figure 2, are used to determine the mean inlet and exit static pressures.

The primary dynamic data quantify the complex unsteady surface pressures on the oscillating cascaded airfoils. These data are obtained via six Kulite dynamic pressure transducers flush mounted symmetrically about the midchord of one surface of the airfoil, Table 1. These transducers, having an active sensor diameter of 0.097 cm (1.3% of the airfoil chord), are placed in milled slots and potted in RTV for isolation from airfoil strain. For the influence coefficient experiments, a thin coating of RTV protects the sensor surface and fairs it into the surface contour of the airfoil.

During oscillation, the RTV-coated pressure transducers are subject to accelerations which may produce significant apparent pressure signals. This effect was quantified by oscillating the instrumented airfoil under no-flow or zero mean velocity conditions. The response of each transducer was found to be a linear function of the acceleration, implying that the acoustic response, which is expected to vary with the airfoil velocity magnitude, is dominated by the acceleration response. Thus calibration data were obtained which could be used to correct the oscillating airfoil data for acceleration effects.

The time-variant position of the reference oscillating airfoil is determined by a capacitance-type proximity sensor which produces a voltage proportional to the air gap between it and an adjacent object. This sensor is positioned to face a six cycle sinusoidally-shaped cam mounted on the airfoil drive camshaft so as to be in phase with the reference airfoil motion.

Data Acquisition and Analysis

Conventional instrumentation is used to quantify the steady flow field. An average of the upstream sidewall static pressures along with the atmospheric pressure are used to calculate the inlet Mach number. Steady flow airfoil surface static pressures are calculated from an average of approximately 100 samples.

Unsteady signals are a.c. coupled and recorded on magnetic tape for post-experiment processing. During tape playback, the signals are simultaneously digitized at rates sufficient to capture at least three harmonics of the oscillation frequency, with 32,768 samples taken per channel. Each data channel is divided into blocks, typically with 4096 samples, and then Fourier decomposed and referenced to the airfoil motion by subtracting the motion phase from the unsteady pressure phase. With all of the transducer signal blocks decomposed, the results are averaged and, for the influence coefficient data, the acceleration responses are subtracted vectorally. To minimize errors due to spectral leakage, an interpolation scheme is applied to the decomposed results in conjunction with a Hanning window [12].

Figure 3 illustrates upper airfoil surface pressure transducer signals from the Mach 0.8 transonic influence coefficient experiment. At 12% of chord, an oscillating shock wave causes a highly non-sinusoidal variation of pressure with time; the averaged pressure spectrum reflects this with a large spike at the oscillation frequency, 350 Hz, and two prominent higher harmonics. At the other transducer locations, the time signals are much more sinusoidal in shape, and the corresponding spectra have only one significant spike located at the oscillation frequency.

Final unsteady pressure data are defined by the complex dynamic pressure and pressure difference coefficients, C_p and ΔC_p, Equation 2.

$$C_p(x) = \frac{p_1(x)}{1/2\rho V^2 \alpha_1} \quad ; \quad \Delta C_p = C_{pl} - C_{pu} \qquad (2)$$

where p_1 is the first harmonic of the unsteady static pressure, α_1 is the torsional oscillation amplitude and C_{pl} and C_{pu} are the lower and upper airfoil surface unsteady pressure coefficients. Dynamic pressure coefficients for any interblade phase angle are determined by summing influence coefficients per Equation 1.

Results

The oscillating cascade aerodynamics are experimentally investigated at subsonic and transonic steady flow conditions defined by an incidence angle of 7 degrees and inlet Mach numbers of 0.65 and 0.80. With the instrumented (reference) airfoil in position 0 as defined in Figure 1, influence coefficient data are acquired on this

airfoil with the airfoils in positions -2, -1, 0, 1 and 2 individually oscillating at reduced frequencies of 0.223 and 0.390 for M=0.65 and 0.185 and 0.323 for M=0.8.

The steady airfoil surface pressure distributions are presented first, then the unsteady pressure influence coefficients on the individual surfaces of the reference instrumented airfoil are considered. These influence coefficient data are then summed to predict the unsteady aerodynamics of an equivalent cascade with all airfoils oscillating at a fixed interblade phase angle value. For several different interblade phase angles, these resulting unsteady pressure distributions are correlated with: (1) baseline data obtained in experiments in which all of the airfoils were simultaneously oscillating at interblade phase angles of -90, 0 and 90 degrees; (2) predictions from the classical unsteady, small perturbation, subsonic, zero mean incidence flat plate analyses of references 13 and 14. Additional interblade phase angle results are obtained utilizing the influence coefficient technique and correlated with the flat plate cascade predictions. In these experiments, the airfoil motion is defined by the change in the incidence angle with time:

$$\alpha(t) = \alpha_0 + \alpha_1 Re\{e^{(i\omega t)}\} \qquad (3)$$

where α_0 is the steady incidence angle, α_1 is the oscillatory amplitude of 1.2 degrees and ω is the frequency.

Steady State Aerodynamics

To demonstrate periodicity at the steady state conditions, airfoil surface pressure distributions are obtained for multiple passages in the cascade. For example, Figure 4 presents data at M=0.8 for the four cascade passages surrounding the center airfoil. Passage 1 data are the pressure distributions for the airfoil 0 (the center airfoil) upper surface and the airfoil 1 lower surface; passage -1 data are for the airfoil 0 lower surface and the airfoil -1 upper surface, etc. The good cascade periodicity is readily apparent. Similar results were obtained for M=0.65.

Figure 5 presents the steady flow airfoil surface pressure coefficient distributions for the center airfoil. As shown, the pressure coefficient distributions are nearly identical for the two Mach numbers, with loading only on the forward half. At Mach 0.8, there is a small region of supersonic flow on the upper surface near the leading edge. The supersonic region is terminated by a shock, as determined from schlieren images.

Data from the taps used to indicate spanwise uniformity are indicated by the darkened symbols. In general, good spanwise uniformity is achieved although there are variations near the leading edge of the airfoil upper surface.

Airfoil Surface Unsteady Pressure Influence Coefficients

Figures 6 through 10 present the chordwise distributions of the first harmonic dynamic pressure influence coefficients on the individual surfaces of the position 0 reference airfoil for M=0.8, with the oscillating airfoil in the five relative positions defined by -2 through 2.

The self-induced oscillating airfoil unsteady pressure response is shown in Figure 6. Namely, this presents the unsteady pressures on the surfaces of the reference airfoil with only the reference airfoil itself oscillating. The magnitude of the unsteady pressure on each surface attains a maximum near the leading edge and tends toward zero at the trailing edge. The largest unsteady pressure magnitude is measured on the upper surface at 12% of chord and is due to the oscillating shock wave. With the exception of the leading transducer data, the unsteady pressure on the upper surface is out of phase with respect to the airfoil motion.

Figures 7 and 8 show the unsteady pressure effect on the surfaces of the stationary instrumented reference airfoil due to individually oscillating its neighbors, i.e., individually oscillating the airfoils in positions 1 and -1, respectively. As shown, oscillating the adjacent neighboring airfoil has a relatively large effect on the magnitude of the unsteady pressure on the reference airfoil surface nearest to the oscillating airfoil. In particular, Figure 7 shows that oscillating the airfoil immediately above the reference airfoil results in relatively large unsteady pressure fluctuations over the reference airfoil upper surface, with the lower surface unsteady pressure coefficient magnitude nearly constant with chord. The phase is nearly constant across the upper surface but varies linearly on the lower surface. With the oscillating airfoil positioned immediately beneath the reference airfoil, Figure 8, there are relatively large pressure fluctuations over the leading quarter of the reference airfoil lower surface, while the upper surface has only a small response in the leading edge region. The lower surface unsteady pressure oscillations are out-of-phase with respect to the airfoil motion.

The effects of oscillating the airfoils in positions 2 and -2 on the unsteady pressure on the surfaces of the instrumented reference airfoil are shown in Figures 9 and 10, respectively. As expected, with the oscillating airfoils further distanced from the reference airfoil, the magnitude of the unsteady pressures on the reference airfoil generally are reduced compared to the previous results. One exception to this is $\hat{C}_p^2$ on the lower surface, which is only slightly reduced in magnitude in comparison to $\hat{C}_p^1$.

Unsteady Pressure Differences

Summation of the unsteady pressure influence coefficients to determine the unsteady pressure difference coefficient is demonstrated in Figure 11. The 0.65 inlet Mach number, 0.39 reduced frequency data are presented as a dynamic pressure difference coefficient for an interblade phase angle of 0 degrees, with N specifying the limits of the sum per Equation 1. Thus N = 0 corresponds to the self-induced unsteady aerodynamic response. The influence coefficient series is rapidly convergent, with only the reference airfoil and its two immediate neighbors having a significant effect on the resulting dynamic pressure differences.

The influence coefficient determined unsteady airfoil surface pressure difference data are correlated with: (1) corresponding data obtained in experiments in which all of the cascaded airfoils are oscillating simultaneously with constant interblade phase angle values of -90, 0 and 90 degrees, and (2) the flat plate cascade predictions. For an inlet Mach number of 0.65, Figures 12, 13 and 14 present the results for a reduced frequency value of 0.223, with the results for a reduced frequency of 0.39 presented in Figures 15, 16 and 17. For an inlet Mach number of 0.80, the unsteady pressure difference results are presented in Figures 18 through 23 for reduced frequencies of 0.185 and 0.323.

There is generally very good magnitude agreement among the two sets of experimental data for all the conditions with the exception of the leading edge region. There, the magnitudes of the influence coefficient data are significantly larger than the others. At M = 0.65, this is due to a small, oscillating separation bubble which was present near the leading edge of the upper surface during the influence coefficient experiments; the presence of separation was first indicated by significant higher harmonic content in the leading upper surface pressure transducer signal, then steady state flow visualization with airfoil 0 at 8.2 degrees of incidence indicated a small separated region near the leading edge. The oscillating leading edge shock is the cause at M = 0.8. Also, for both inlet Mach numbers, the theory tends to overpredict the magnitude, particularly at the lower reduced frequencies.

The two sets of experimental unsteady pressure difference phase angle data often are in good agreement. However, this agreement varies, with the interblade phase angle and inlet Mach number having the most significant effects. For $\beta = -90°$, the influence coefficient data are in good agreement with the data for all airfoils oscillating and also the predictions. For $\beta = 90°$ and M = 0.65, all of the phase angle data fall within a fairly narrow band, with the influence coefficient results typically between the prediction and the data for all airfoils oscillating. This trend is also evident for M = 0.8 and $\beta = 90°$ although there is more offset among the various results, particularly for k = 0.323. Correlation of the experimental phase angle data for in-phase motions is good at M = 0.65 but scattered at M = 0.8; at both inlet Mach numbers, there is better agreement between the experimental data and the predictions at the lower reduced frequencies.

Airfoil surface unsteady pressure difference distributions for interblade phase angle values of -45, 45 and 180 degrees are correlated with the theory for both reduced frequency values with M = 0.8, Figures 24 and 25. For k = 0.185, Figure 24, the predicted magnitudes are significantly larger than the data. The magnitude correlation is improved at the higher reduced frequency, although the theoretical values are still generally larger in value than the data, Figure 25. The phase angle data-theory correlation for out-of-phase oscillations is very good for both reduced frequencies. For $\beta = -45°$, the phase angle agreement is good except at 25% of chord. Finally, at $\beta = 45°$, the correlation is not very good.

Summary and Conclusions

Fundamental experiments have been performed in the NASA Lewis Transonic Oscillating Cascade Facility to investigate the steady and torsion mode oscillating aerodynamics of a biconvex airfoil cascade. For subsonic and transonic mean flow conditions, and realistic high values of reduced frequency, an unsteady aerodynamic influence coefficient technique was utilized in which only one airfoil in the cascade is oscillated at a time and the resulting unsteady pressures measured on the oscillating airfoil and its stationary neighbors. Vector summation of these data allows determination of the unsteady aerodynamics for arbitrary interblade phase angles of an equivalent cascade with all airfoils oscillating.

Analysis of these unique data and correlation with both the predictions from the unsteady, small perturbation, subsonic flat plate cascade analyses and the baseline data obtained in experiments where all of the airfoils are oscillating simultaneously revealed the following.

* The unsteady aerodynamic influence coefficient series is rapidly convergent, with only the reference airfoil and its two neighbors having a significant effect on the resulting unsteady pressure difference.

* The complex unsteady pressure difference influence coefficient data generally exhibit good correlation with both the oscillating cascade data and the linearized theory, except in the vicinity of the leading edge.

* As the reduced frequency decreases, the linearized theory tends to overpredict the magnitude of the unsteady pressure difference.

In summary, this unsteady aerodynamic influence coefficient experimental technique allows valid oscillating cascade data to be obtained in regions of subsonic, attached flow at realistic values of reduced frequency for all interblade phase angle values.

References

1. Atassi, H. and Akai, T.J., "Aerodynamic and Aeroelastic Characteristics of Oscillating Loaded Cascades at Low Mach Number," *ASME Paper 79-GT-111*, March 1979.
2. Whitehead, D.S., "The Calculation of Steady and Unsteady Transonic Flow in Cascades," *Cambridge University Report CUED/A-Turbo/TR118*, 1982.
3. Verdon, J.M. and Caspar, J.R., "A Linearized Unsteady Aerodynamic Analysis for Transonic Cascades," *Journal of Fluid Mechanics*, Vol. 149, December 1984.
4. Usab, W.J. and Verdon, J.M., "On the Application of a Linearized Unsteady Potential Flow Analysis to Fan-Tip Cascades," *ASME Paper 86-GT-87*, June 1986.
5. Chiang, H.D. and Fleeter, S., "Locally Analytical Numerical Method for Inviscid Oscillating Airfoil Aerodynamics," Presented at the *SIAM 1986 National Meeting*, Boston, July 1986.
6. Hall, K.C. and Crawley, E.F., "Calculation of Unsteady Flows in Turbomachinery Using the Linearized Euler Equations," *Unsteady Aerodynamics and Aeroelasticity of Turbomachines and Propellers*, Aachen Institute of Technology, Aachen, W. Germany, 1988.
7. Huff, D.L., "Numerical Simulation of Unsteady, Viscous, Transonic Flow Over Isolated and Cascaded Airfoils Using a Deforming Grid Technique," *NASA Technical Memorandum 89890, AIAA Paper 87-1316*, June 1987.
8. Hanamura, Y., Tanaka, H. and Yamaguchi, K., "A Simplified Method to Measure Unsteady Forces Acting on the Vibrating Blades in Cascade," *Bulletin of the JSME*, Vol. 23, No. 180, June 1980.
9. Davies, M.R.D. and Whitehead, D.S., "Unsteady Aerodynamic Measurements in a Transonic Annular Cascade," *Unsteady Aerodynamics of Turbomachines and Propellers*, Cambridge University, Cambridge, England, 1984.
10. Tanaka, H., Yamamoto, K. and Fujimoto, I., "Unsteady Aerodynamic Response of Cascade Blades in Pitching Oscillation with Flow Separation," *Unsteady Aerodynamics of Turbomachines and Propellers*, Cambridge University, Cambridge, England, 1984.
11. Buffum, D.H. and Fleeter, S., "Investigation of Oscillating Cascade Aerodynamics by an Experimental Influence Coefficient Technique," *NASA Technical Memorandum 101313, AIAA Paper 88-2815*, July 1988.
12. Burgess, J.C., "On Digital Spectrum Analysis of Periodic Signals," *Journal of the Acoustical Society of America*, Vol. 58, No. 3, September 1975.
13. Smith, S.N., "Discrete Frequency Sound Generation in Axial Flow Turbomachines," *Cambridge University Report CUED/A-Turbo/TR29*, 1971.
14. Fleeter, S., "Fluctuating Lift and Moment Coefficients for Cascaded Airfoils in a Nonuniform Compressible Flow," *AIAA Journal of Aircraft*, Vol. 10, No. 2, February 1973.

Table 1. Airfoil and cascade geometry

AIRFOIL	
Type	biconvex, no camber
Surface radius of curvature	27.4 cm
Leading and trailing edge radii of curvature	0.025 cm
Maximum airfoil thickness	0.58 cm
Chord, C	7.62 cm
Elastic axis	midchord
Dynamic pressure transducer locations, % chord	12, 25, 40, 60, 75, 88
CASCADE	
Number of airfoils	9
Solidity, C/S	1.3
Spacing, S	5.86 cm
Stagger angle, γ	53 degrees
Amplitude of motion	1.2 degrees

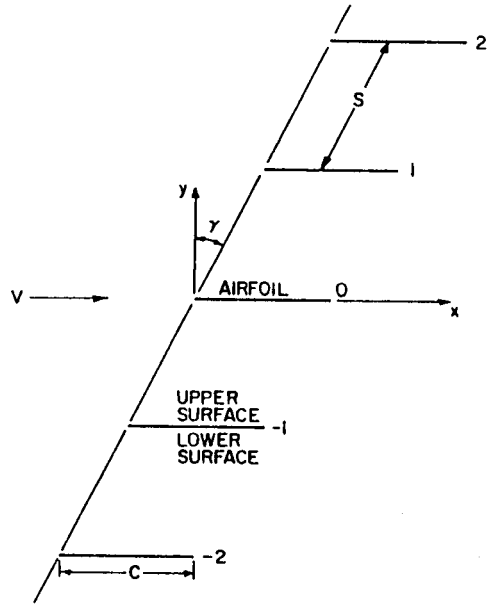

Figure 1. Cascade geometry

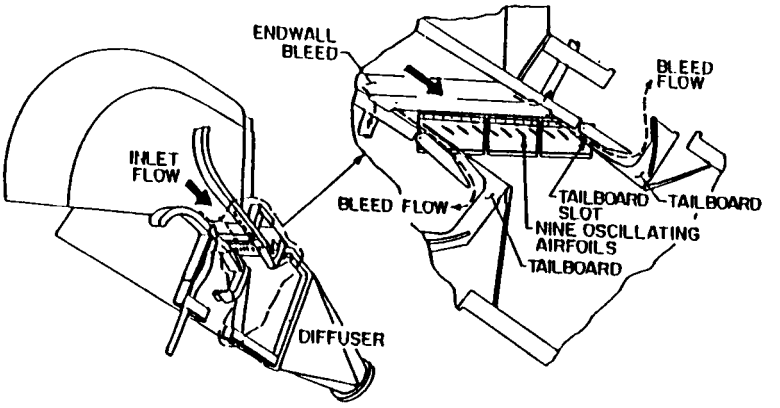

Figure 2. NASA Lewis Transonic Oscillating Cascade Facility

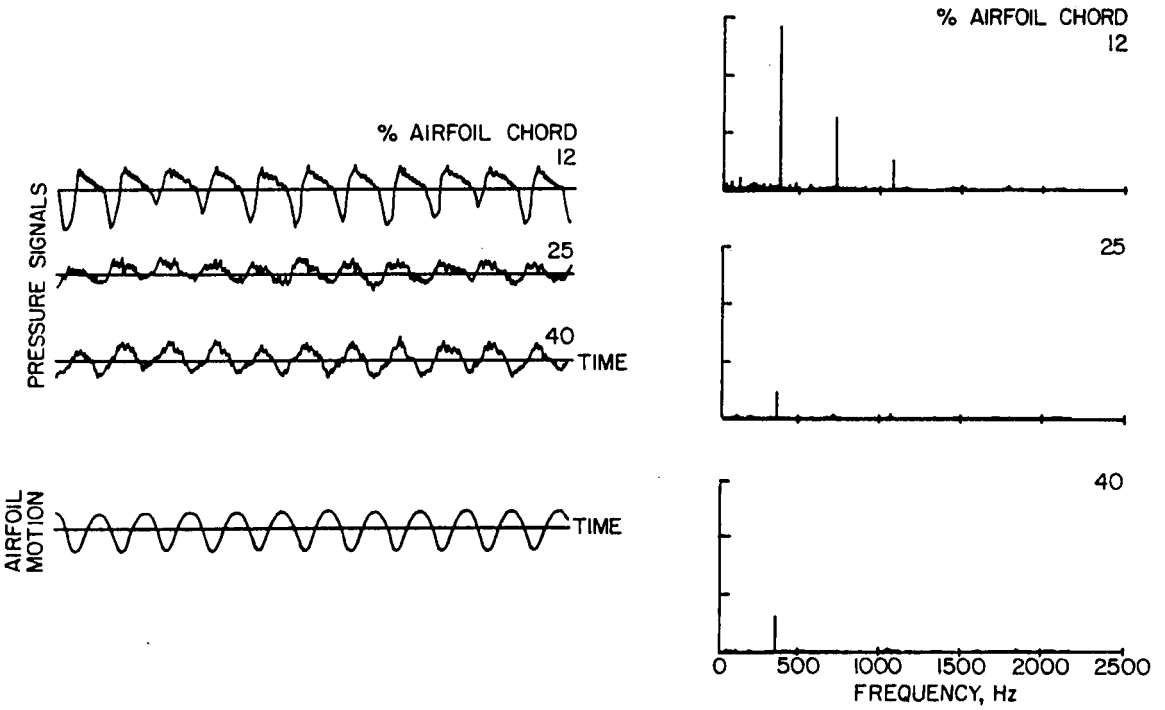

Figure 3. Time-variant signals and averaged pressure spectra, M = 0.80, k = 0.323

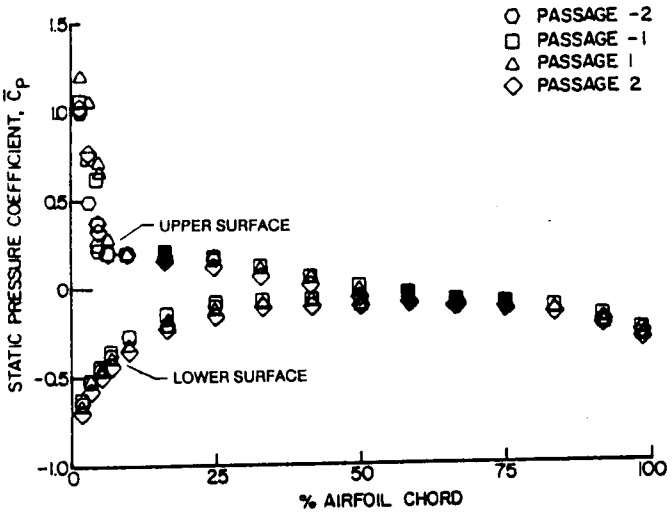

Figure 4. Periodicity of steady flow airfoil surface pressure distribution, M = 0.80

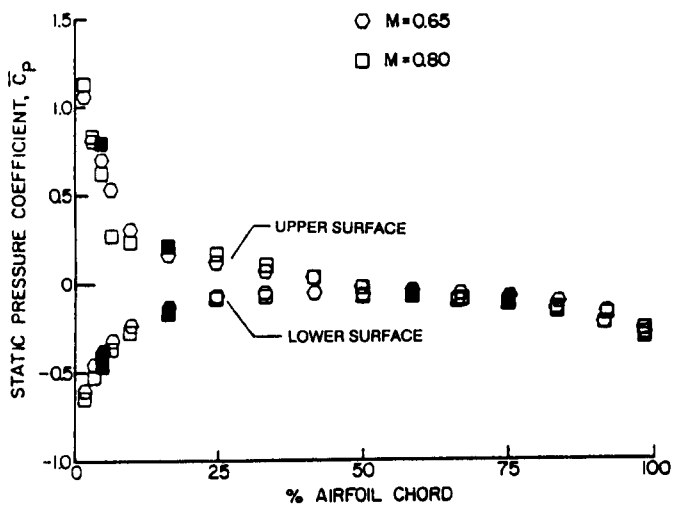

Figure 5. Steady flow airfoil surface pressure distribuitions

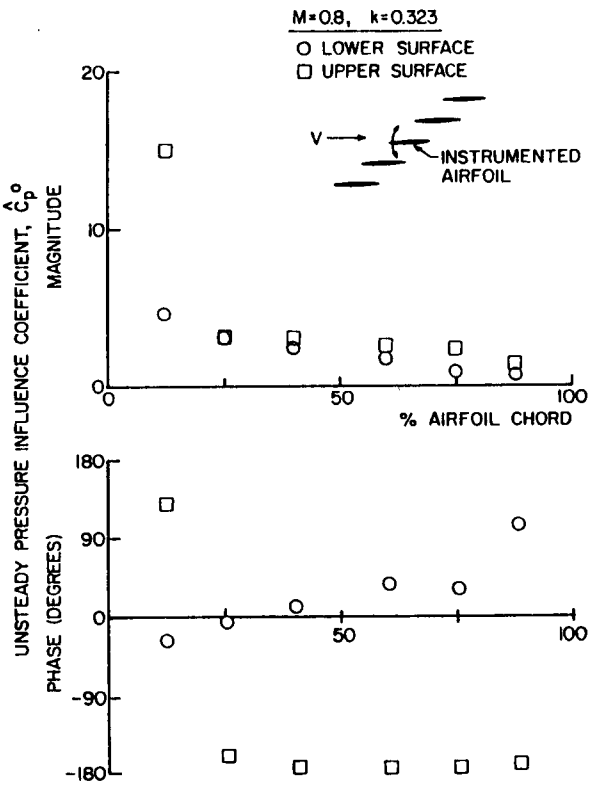

Figure 6. Unsteady pressure influence coefficient, airfoil 0 oscillating

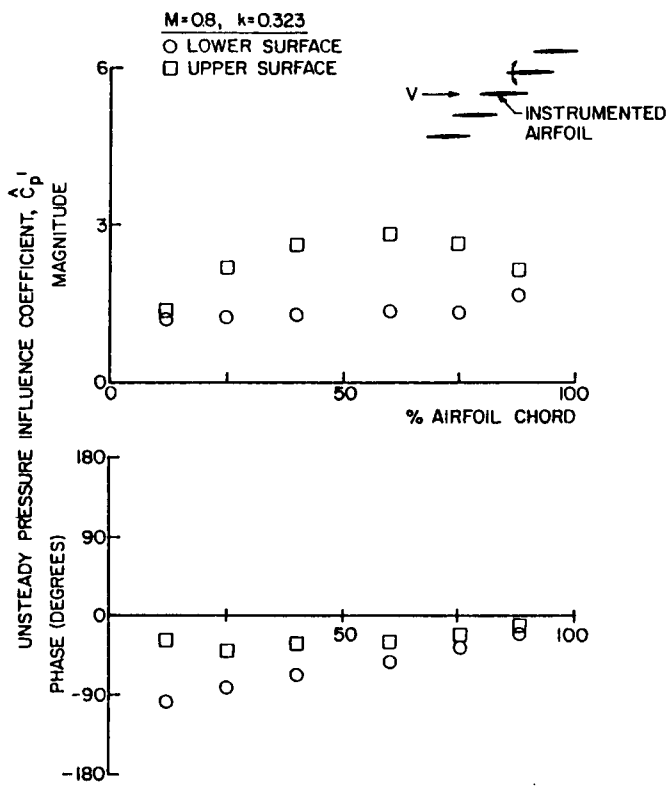

Figure 7. Unsteady pressure influence coefficient, airfoil 1 oscillating

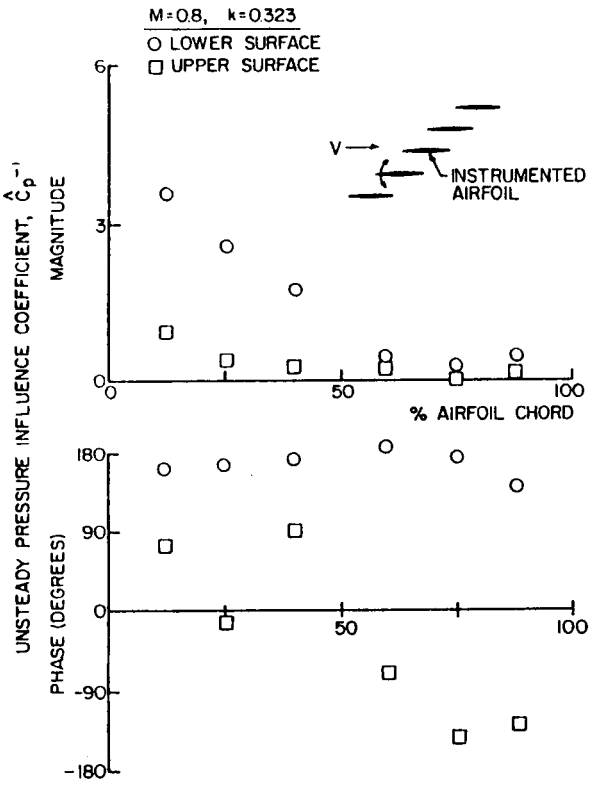

Figure 8. Unsteady pressure influence coefficient, airfoil -1 oscillating

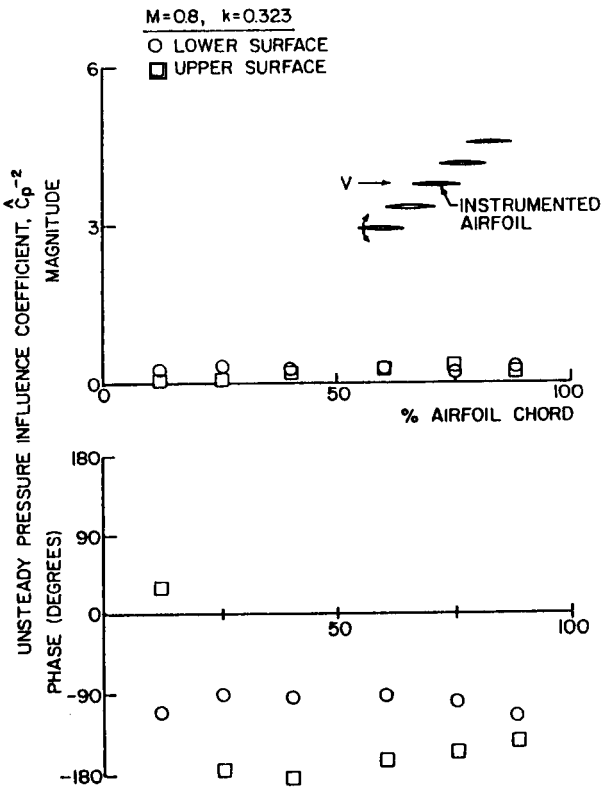

Figure 10. Unsteady pressure influence coefficient, airfoil -2 oscillating

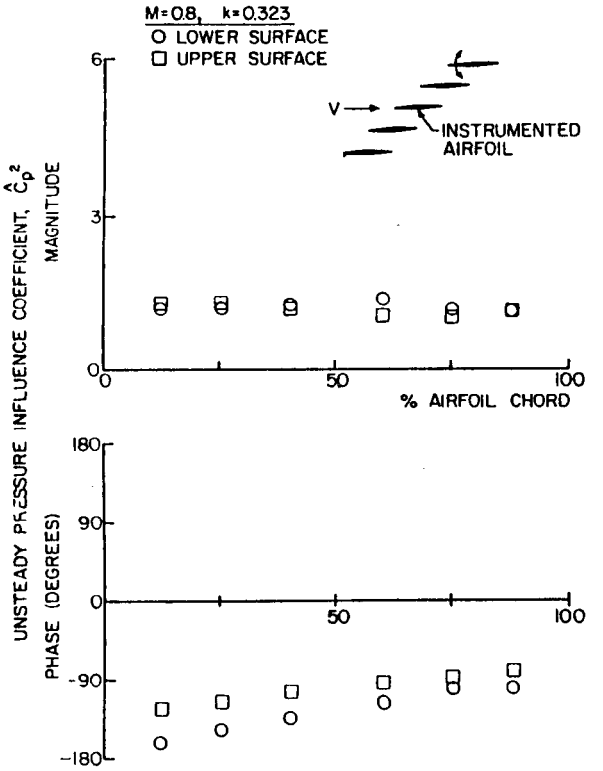

Figure 9. Unsteady pressure influence coefficient, airfoil 2 oscillating

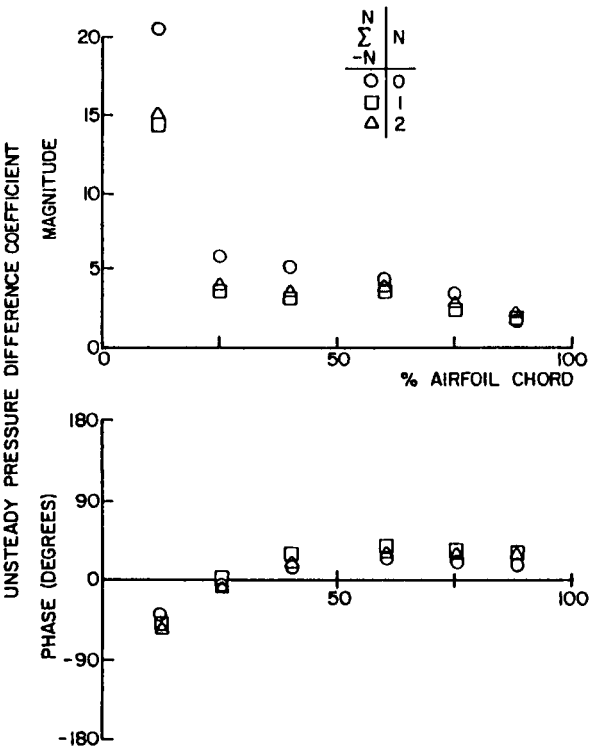

Figure 11. Summation of unsteady pressure influence coefficients, $M = 0.65, k = 0.39, \beta = 0^\circ$

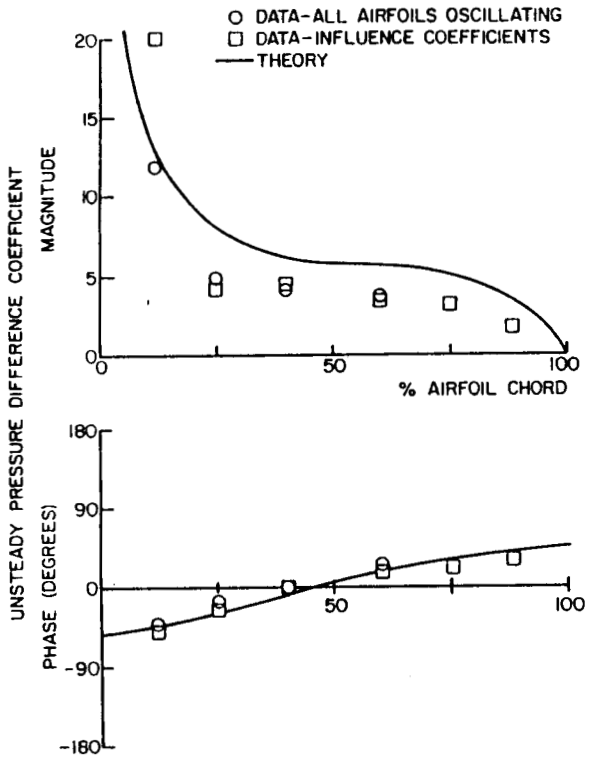

Figure 12. Unsteady pressure difference coefficient distribution, $M = 0.65, k = 0.223, \beta = -90°$

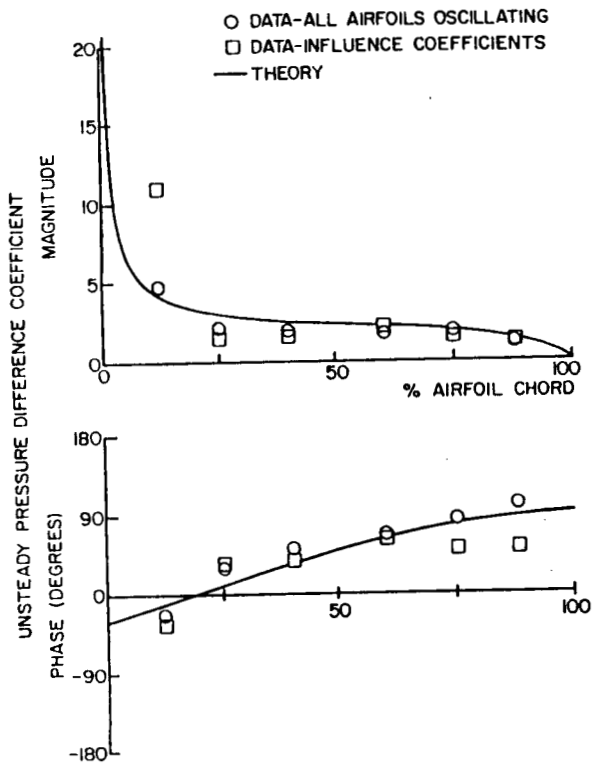

Figure 13. Unsteady pressure difference coefficient distribution, $M = 0.65, k = 0.223, \beta = 0°$

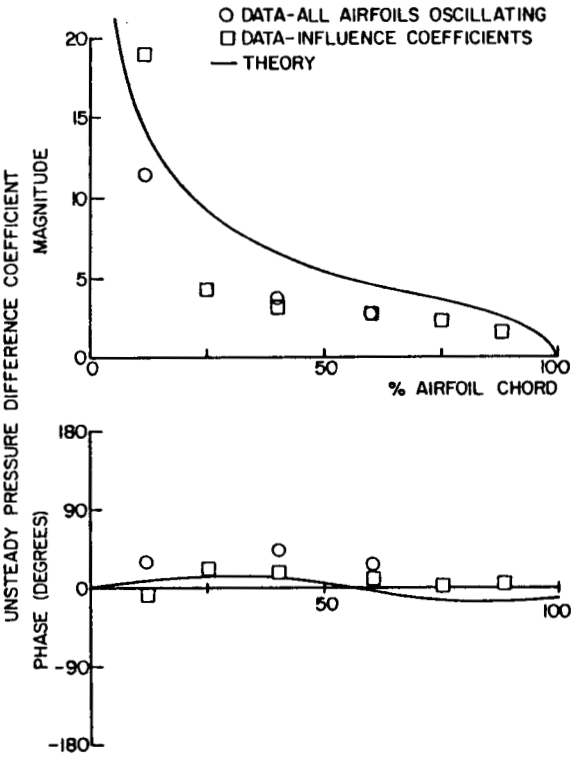

Figure 14. Unsteady pressure difference coefficient distribution, $M = 0.65, k = 0.223, \beta = 90°$

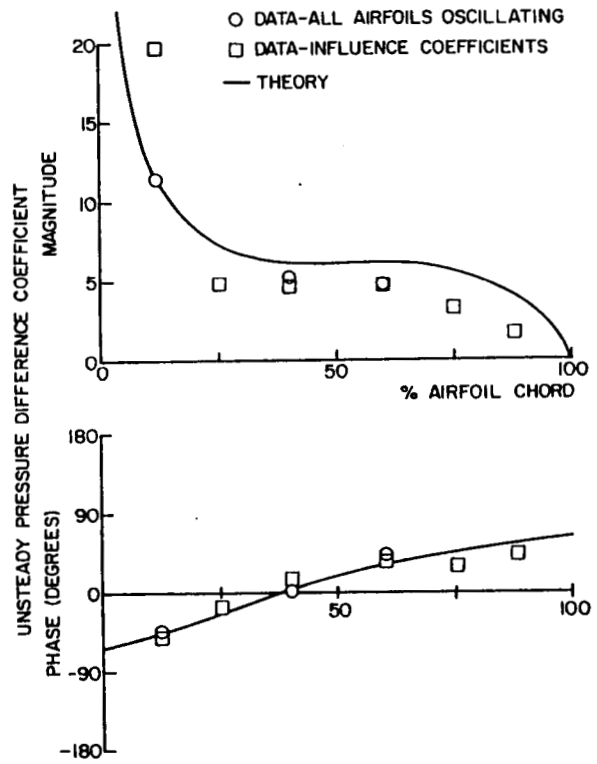

Figure 15. Unsteady pressure difference coefficient distribution, $M = 0.65, k = 0.39, \beta = -90°$

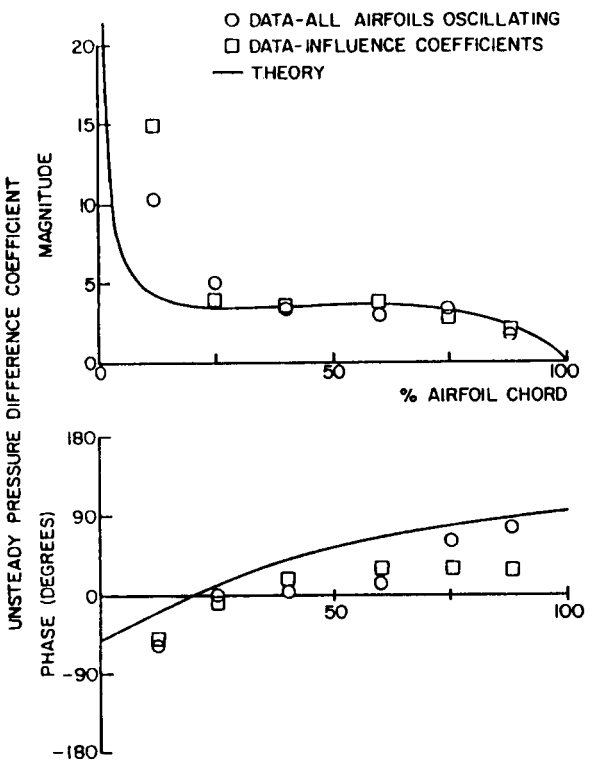

Figure 16. Unsteady pressure difference coefficient distribution, $M = 0.65, k = 0.39, \beta = 0°$

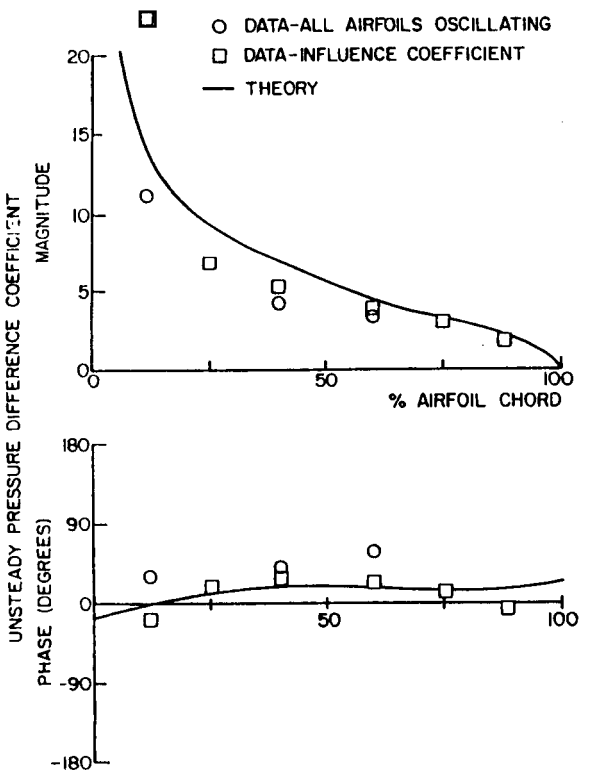

Figure 17. Unsteady pressure difference coefficient distribution, $M = 0.65, k = 0.39, \beta = 90°$

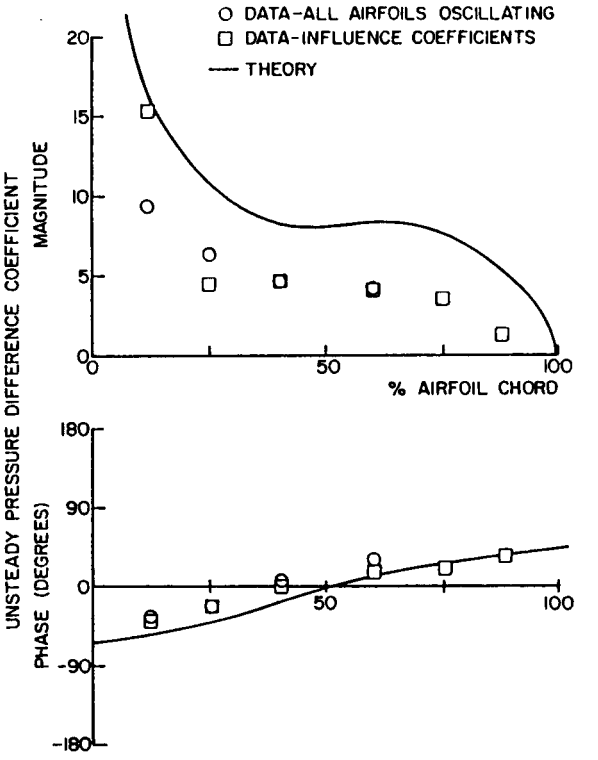

Figure 18. Unsteady pressure difference coefficient distribution, $M = 0.80, k = 0.185, \beta = -90°$

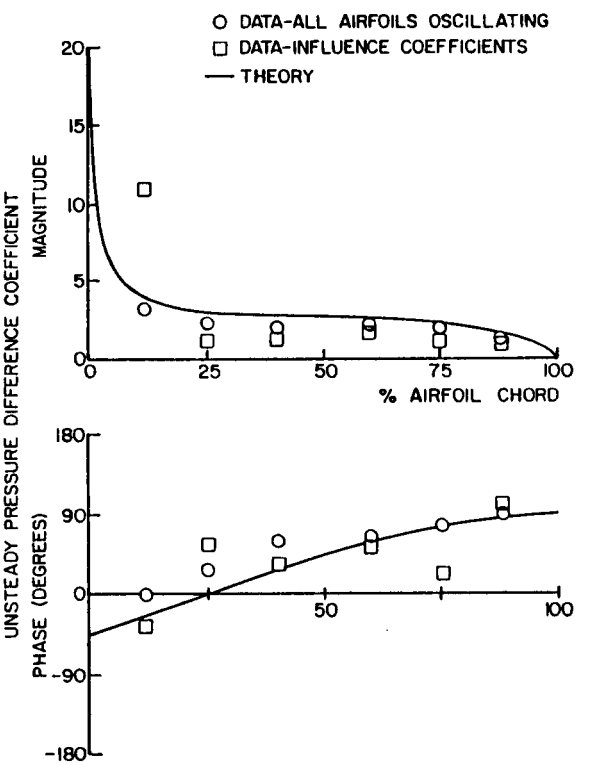

Figure 19. Unsteady pressure difference coefficient distribution, $M = 0.80, k = 0.185, \beta = 0°$

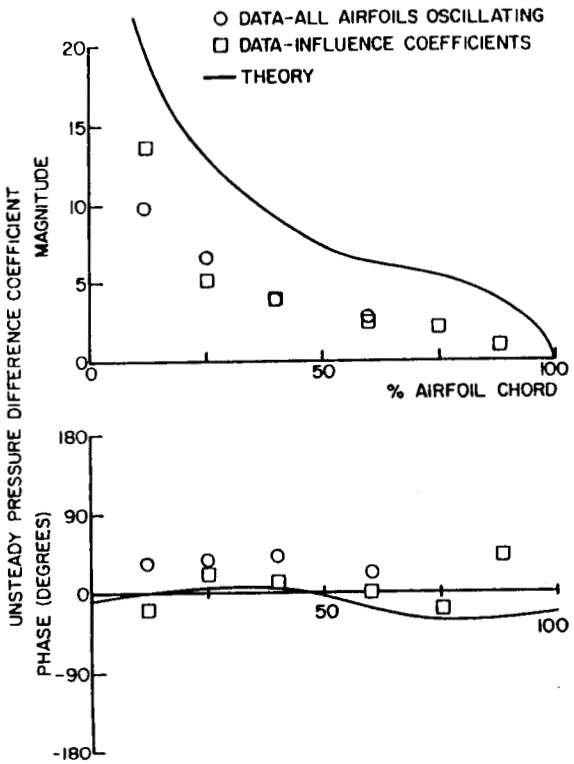

Figure 20. Unsteady pressure difference coefficient distribution, $M = 0.80, k = 0.185, \beta = 90°$

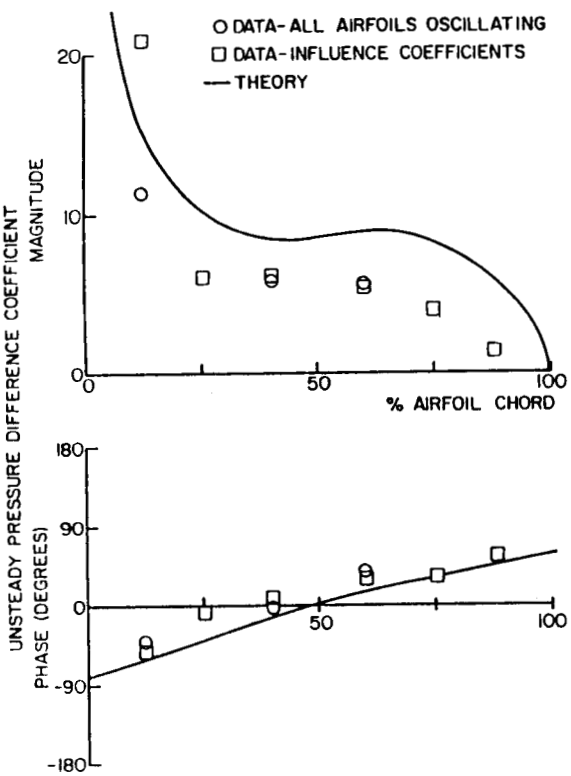

Figure 21. Unsteady pressure difference coefficient distribution, $M = 0.80, k = 0.323, \beta = -90°$

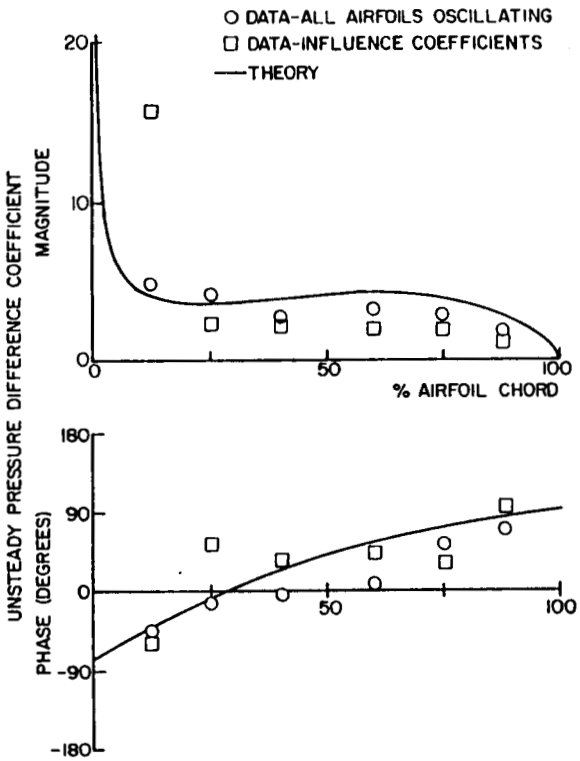

Figure 22. Unsteady pressure difference coefficient distribution, $M = 0.80, k = 0.323, \beta = 0°$

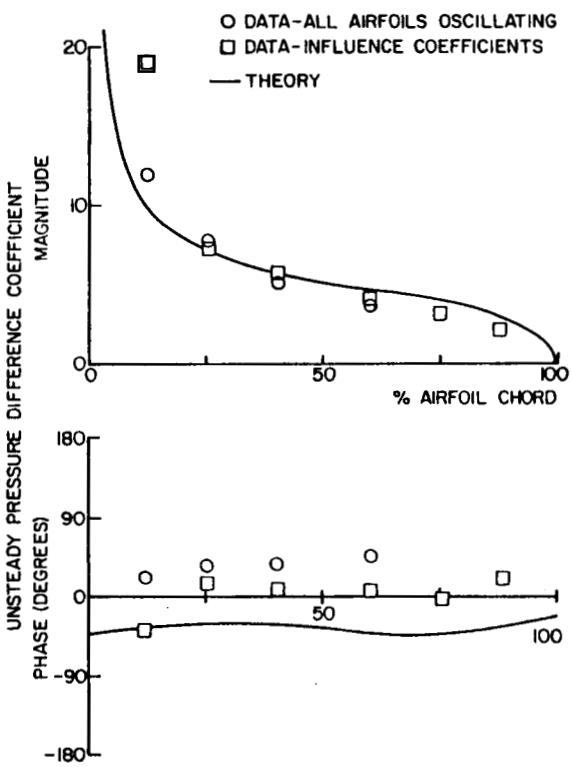

Figure 23. Unsteady pressure difference coefficient distribution, $M = 0.80, k = 0.323, \beta = 90°$

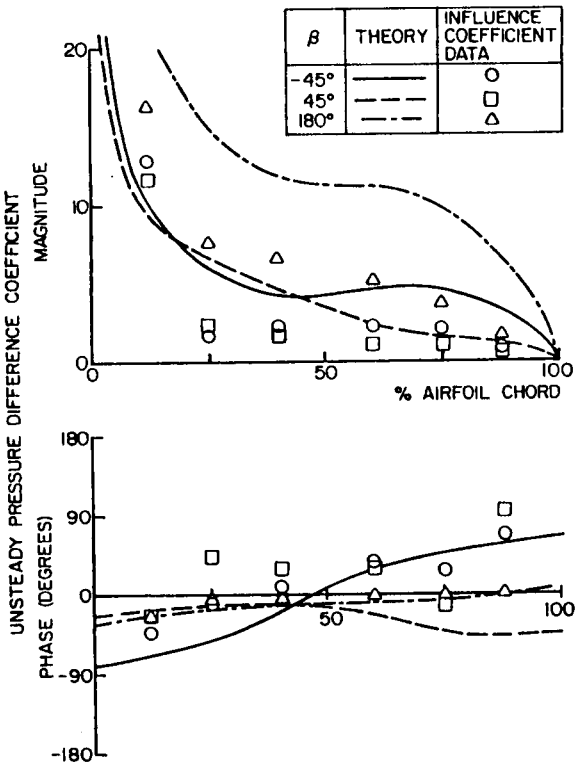

Figure 24. Correlation of unsteady pressure difference coefficient distribution, $M = 0.80$, $k = 0.185$

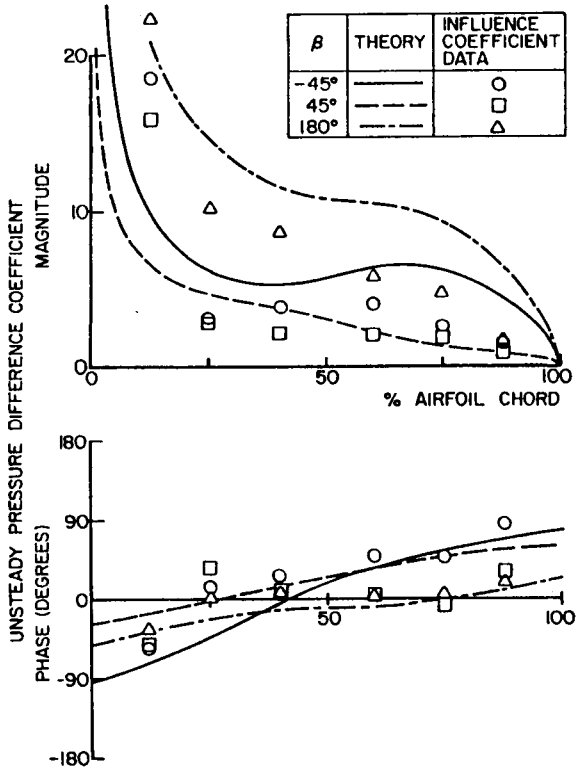

Figure 25. Correlation of unsteady pressure difference coefficient distribution, $M = 0.80$, $k = 0.323$

NASA
National Aeronautics and Space Administration

Report Documentation Page

1. Report No.	2. Government Accession No.	3. Recipient's Catalog No.
NASA TM-101993		

4. Title and Subtitle	5. Report Date
Experimental Investigation of Transonic Oscillating Cascade Aerodynamics	6. Performing Organization Code

7. Author(s)	8. Performing Organization Report No.
Daniel H. Buffum and Sanford Fleeter	E-4697
	10. Work Unit No. 505-62-61

9. Performing Organization Name and Address	11. Contract or Grant No.
National Aeronautics and Space Administration Lewis Research Center Cleveland, Ohio 44135-3191	13. Type of Report and Period Covered Technical Memorandum
12. Sponsoring Agency Name and Address	14. Sponsoring Agency Code
National Aeronautics and Space Administration Washington, D.C. 20546-0001	

15. Supplementary Notes

Prepared for the 27th Aerospace Sciences Meeting sponsored by the American Institute of Aeronautics and Astronautics, Reno, Nevada, January 9-12, 1989. Daniel H. Buffum, NASA Lewis Research Center; Sanford Fleeter, Thermal Sciences and Propulsion Center, School of Mechanical Engineering, Purdue University, West Lafayette, Indiana 47907 (work funded by NASA Grant NAG3-656).

16. Abstract

Fundamental experiments are performed in the NASA Lewis Transonic Oscillating Cascade Facility to investigate the subsonic and transonic aerodynamics of cascaded airfoils executing torsion mode oscillations at realistic values of reduced frequency. In particular, an unsteady aerodynamic influence coefficient technique is developed and utilized. In this technique, only one airfoil in the cascade is oscillated at a time, with the resulting airfoil surface unsteady pressure distribution measured on one dynamically instrumented reference airfoil. The unsteady aerodynamics of an equivalent cascade with all airfoils oscillating at any specified interblade phase angle are then determined through a vector summation of these data. These influence coefficient determined oscillating cascade data were correlated with: (1) data obtained in this cascade with all airfoils oscillating at several interblade phase angle values; (2) predictions from a classical linearized unsteady cascade model.

17. Key Words (Suggested by Author(s))	18. Distribution Statement
Cascades Oscillating cascades Unsteady aerodynamics Flutter	Unclassified – Unlimited Subject Category 07

19. Security Classif. (of this report)	20. Security Classif. (of this page)	21. No of pages	22. Price*
Unclassified	Unclassified	15	A03

*For sale by the National Technical Information Service, Springfield, Virginia 22161